

Effects of coupling to breakup in the ${}^6,{}^7\text{Li} + {}^{64}\text{Zn}$ systems at near-barrier energies

J. P. Fernández-García,^{1,*} M. Zadro,² A. Di Pietro,¹ P. Figuera,¹ M. Fisichella,¹ O. Goryunov,³ M. Lattuada,^{1,4} C. Marchetta,¹ A. M. Moro,⁵ A. Musumarra,^{1,4} V. Ostashko,³ M. G. Pellegriti,^{1,4} V. Scuderi,^{1,4} E. Strano,^{1,4} and D. Torresi^{1,4}

¹*INFN, Laboratori Nazionali del Sud, via S. Sofia 62, I-95123 Catania, Italy*

²*Ruđer Bošković Institute, Bijenička cesta 54, HR-10000 Zagreb, Croatia*

³*Institute for Nuclear Research, Prospekt Nauki, UA-03680 Kiev, Ukraine*

⁴*Dipartimento di Fisica e Astronomia, via S. Sofia 64, I-95123 Catania, Italy*

⁵*Departamento de FAMN, Universidad de Sevilla, Apartado 1065, E-41080 Seville, Spain*

(Received 13 May 2015; revised manuscript received 8 October 2015; published 3 November 2015)

Elastic scattering angular distributions for the weakly bound nucleus ${}^7\text{Li}$ on ${}^{64}\text{Zn}$ have been measured in a wide angular range at energies around the Coulomb barrier. The present experimental data and our previously measured elastic scattering data for the system ${}^6\text{Li} + {}^{64}\text{Zn}$ have been analyzed within the continuum-discretized coupled-channels method, where the resonant and nonresonant states of the projectile are taken into account. In this theoretical framework, we have also analyzed our previously measured excitation functions of elastic scattering at backward angles and the corresponding barrier distributions for the same systems. A good agreement between the experimental data and the calculations has been observed. The obtained results, besides confirming the importance of the coupling to the breakup channels in collisions with weakly bound nuclei, show that, in the case of ${}^6\text{Li}$, the inclusion of the resonant states of the projectile produces non-negligible effects.

DOI: [10.1103/PhysRevC.92.054602](https://doi.org/10.1103/PhysRevC.92.054602)

PACS number(s): 25.70.Bc, 25.70.Mn, 24.10.Eq

I. INTRODUCTION

In the last decade, many efforts have been concentrated on the study of nuclear collisions at energies around the Coulomb barrier induced by stable weakly bound nuclei, such as ${}^6\text{Li}$ and ${}^7\text{Li}$ (see, e.g., Ref. [1] and references therein). ${}^6\text{Li}$ and ${}^7\text{Li}$ nuclei have weakly bound cluster structures, i.e., ${}^6\text{Li} = \alpha + d$ and ${}^7\text{Li} = \alpha + t$, with separation energies $S_\alpha = 1.47$ MeV and 2.47 MeV, respectively [2]. Therefore, owing to this peculiarity, the coupling to the breakup channels can affect the dynamics of reactions induced by these nuclei (see, e.g., Refs. [1,3]).

Strong effects of the loosely bound structure on elastic scattering have been found in reactions involving unstable halo nuclei, such as ${}^{11}\text{Be}$, ${}^6\text{He}$, and ${}^{11}\text{Li}$ (see, e.g., Refs. [4–8]). In the case of elastic scattering with stable weakly bound nuclei, these effects were also clearly observed in the energy dependence of the optical potential, where no usual threshold anomaly appears (see, e.g., Refs. [9–15]).

The elastic scattering angular distributions of ${}^6,{}^7\text{Li}$ on different targets have also been extensively investigated within the continuum-discretized coupled-channel (CDCC) framework (see Refs. [16–19]). Couplings to the ${}^6,{}^7\text{Li} \rightarrow \alpha + d(t)$ resonant and nonresonant breakup processes were demonstrated to have a significant effect on the elastic scattering cross section.

The barrier distribution method has been proved to be a powerful tool to study the effects of couplings to different reaction channels at near-barrier energies (see, e.g., Refs. [20,21]). Due to the difficulties to extract the barrier distribution from fusion measurements, an alternative representation can be derived from the quasielastic (QEL) scattering at backward angles. Those two descriptions are

linked through the conservation of the reaction flux, since fusion is connected to the probability of transmission and QEL to the reflection probability. Therefore, the QEL backscattering can be considered as complementary to fusion. The barrier distribution of quasielastic scattering (D_{qel}) is defined as [22]

$$D_{\text{qel}}(E) = -\frac{d}{dE} \left[\frac{d\sigma_{\text{qel}}}{d\sigma_{\text{Ruth}}} \right], \quad (1)$$

where $d\sigma_{\text{qel}}/d\sigma_{\text{Ruth}}$ corresponds to the ratio of the quasielastic scattering and the Rutherford differential cross sections at a fixed backward angle. QEL scattering is defined as the sum of elastic and inelastic scattering, and all other direct processes.

Another representation of the barrier distribution can be obtained from the elastic backscattering excitation function (see, e.g., Ref. [23]).

It has been shown for several systems that the barrier distributions derived from quasielastic scattering (and elastic, in the case of tightly bound nuclei) are similar to those derived from fusion (see, e.g., Refs. [24–26]). In reactions with weakly bound nuclei, if only the elastic and inelastic cross sections are included in the QEL, the D_{qel} distribution does not provide information about the fusion barrier, but it reflects the “total-reaction threshold distribution” [27,28] (see also Refs. [29,30]).

In Refs. [31–35], excitation functions for QEL and/or elastic scattering at backward angles, and the corresponding barrier distributions, have been measured and analyzed for several systems involving ${}^6,{}^7\text{Li}$. The results show that the effects of coupling to breakup channels are larger for ${}^6\text{Li}$ than for ${}^7\text{Li}$.

With the aim of contributing to the investigation of the dynamics of reactions induced by weakly bound nuclei, we have performed a systematic study of the ${}^6,{}^7\text{Li} + {}^{64}\text{Zn}$ systems at energies around the Coulomb barrier where, elastic scattering angular distributions and fusion excitation functions were

*fernandez@lns.infn.it

measured and elastic and QEL barrier distributions derived from the corresponding excitation function measurements [36–38]. In Ref. [36], the elastic scattering of ${}^6\text{Li}$ on ${}^{64}\text{Zn}$ at energies around the Coulomb barrier has been investigated within the optical model. The energy dependence of the optical potential reveals an absence of the usual threshold anomaly [39]. This new kind of anomaly, so-called “breakup threshold anomaly” [12], can be understood as an evidence of the effect of the coupling to the breakup channels.

Moreover, in [37], elastic and QEL barrier distributions were analyzed within the coupled-channel approach including inelastic excitations of the projectile and target. These calculations did not reproduce the experimental data in the case of ${}^6\text{Li}$ projectile. This result suggests that the effects of couplings to the continuum will be important in the reactions induced by ${}^6\text{Li}$.

In order to conclude our systematic study of ${}^{6,7}\text{Li} + {}^{64}\text{Zn}$, we measured elastic scattering angular distributions for the ${}^7\text{Li} + {}^{64}\text{Zn}$ system at energies around the Coulomb barrier not measured before and investigated the effects of coupling to breakup in the ${}^{6,7}\text{Li} + {}^{64}\text{Zn}$ systems within the three-body CDCC framework. The new experimental data and those that we previously measured in Ref. [36] for the ${}^6\text{Li} + {}^{64}\text{Zn}$ elastic scattering angular distributions are compared with the CDCC calculations to look for differences in the breakup coupling effects for the two projectiles, ${}^6\text{Li}$ and ${}^7\text{Li}$. Moreover, we investigated the effect of different ${}^6\text{Li}$ resonant states on the elastic scattering angular distributions. Furthermore, we analyzed, in terms of the CDCC calculations, barrier distributions obtained from the backscattering excitation functions reported in Ref. [37] for both ${}^{6,7}\text{Li} + {}^{64}\text{Zn}$ systems. It is also interesting to see whether the elastic scattering angular distributions and the barrier distributions can be described simultaneously by means of the same CDCC calculations. The results of this investigation are reported in the present paper.

This paper is organized as follows. First, in Sec. II, the measurements of the elastic scattering of ${}^7\text{Li}$ on ${}^{64}\text{Zn}$ are presented. The CDCC calculations are described in Sec. III. In Sec. IV, the results of the CDCC calculations are compared with the experimental elastic angular distributions, the backscattering excitation functions, and the barrier distributions for the ${}^{6,7}\text{Li} + {}^{64}\text{Zn}$ systems. The effects of the couplings to breakup channels are discussed. Finally, in Sec. V, a brief summary of our results is presented.

II. EXPERIMENTAL DETAILS AND RESULTS

The measurements of the elastic scattering angular distributions of ${}^7\text{Li}$ on ${}^{64}\text{Zn}$ were performed in two different experiments: in the first experiment the measurements corresponding to higher energies $E_{\text{lab}} = 18.33$ and 20.18 MeV were carried out, while in a second experiment those corresponding to lower energies $E_{\text{lab}} = 13.03, 13.85, 15.08,$ and 16.60 MeV were performed. The measurements were carried out at the Laboratori Nazionali del Sud. The ${}^7\text{Li}$ beam was produced by the SMP Tandem Van de Graaff accelerator and transported to the CT2000 scattering chamber. The target was 99.4% enriched ${}^{64}\text{Zn}$ evaporated onto a carbon backing and placed at 45° with respect to the beam direction. The target thickness

was $140 \mu\text{g}/\text{cm}^2$ on a $60 \mu\text{g}/\text{cm}^2$ carbon backing in the first experiment and $110 \mu\text{g}/\text{cm}^2$ on a $20 \mu\text{g}/\text{cm}^2$ carbon backing in the second experiment. A thin ${}^{209}\text{Bi}$ backing layer, $2\text{--}3 \mu\text{g}/\text{cm}^2$, was also present in the target used in the second experiment. In the data analysis, the beam energies were corrected for the energy loss in the first half of the target.

Charged particles coming from the reactions were detected and identified by five silicon telescopes. Each telescope was composed by a $\sim 10 \mu\text{m}$ thick detector (ΔE) and a detector with a thickness in the range $100\text{--}400 \mu\text{m}$ (E). The telescope system was mounted on a rotating plate in the scattering chamber. The angular separation between adjacent telescopes was 10° . The angular distributions were measured in steps of $2.5^\circ\text{--}10^\circ$, depending on the beam energy and on the angular region, in the angular ranges of $\theta_{\text{lab}} = 30^\circ\text{--}170^\circ$ at lower energies and $\theta_{\text{lab}} = 20^\circ\text{--}135^\circ$ at higher energies. Circular collimators with diameters of 6 mm were positioned in front of each telescope, in such a way that their angular opening with respect to the target center was between 0.8° and 1.0° .

The beam was defined by a rectangular aperture of $3 \times 3 \text{ mm}^2$ and a circular collimator with a diameter of 1 mm, placed 155 cm and 16 cm upstream of the target, respectively.

Two monitor telescopes with angular opening of $\sim 0.2^\circ$, placed at $\pm 12.5^\circ$ in the first experiment, and at $\pm 20^\circ$ in the second experiment, were used for normalization purposes.

Absolute values of the cross sections were obtained by assuming that the ${}^6\text{Li} + {}^{64}\text{Zn}$ scattering at forward angles, where the two monitor detectors were placed, is pure Rutherford. It should be mentioned that the events corresponding to the elastic scattering on ${}^{64}\text{Zn}$ and ${}^{208}\text{Bi}$, which was present in the target of the second experiment, were not separated at these small angles. Therefore, the number of “background” events from ${}^{209}\text{Bi}$ had to be evaluated and subtracted from the elastic scattering counts in the monitor detectors. For that reason, one additional monitor telescope, with angular opening of $\sim 2^\circ$ and placed at $\sim 90^\circ$, was used in the second experiment. The number of counts in the forward monitors corresponding to the scattering on ${}^{209}\text{Bi}$ was then determined from the number of counts in the monitor placed at 90° , by assuming a pure Rutherford scattering of ${}^6\text{Li}$ on ${}^{209}\text{Bi}$ for all monitor detectors.

The ratios of the solid angles between monitors and telescopes were determined by measuring the elastic scattering of ${}^7\text{Li}$ on a $140 \mu\text{g}/\text{cm}^2$ thick gold target (assuming Rutherford scattering). More details of the normalization procedure can be found in Ref. [36].

Figure 1 shows a two-dimensional spectrum ΔE versus residual energy E_{res} measured at $E_{\text{lab}} = 16.6$ MeV with a telescope at 135.2° . Events corresponding to $Z = 1, 2,$ and 3 are well separated. The $Z = 3$ events associated to the elastic scattering and inelastic scattering to the $0.48 \text{ MeV } 1/2^-$ state of ${}^7\text{Li}$ and the $0.99 \text{ MeV } 2^+$ state of ${}^{64}\text{Zn}$, as well as elastic scattering on ${}^{209}\text{Bi}$ are clearly visible. Events corresponding to the ${}^{64}\text{Zn}({}^7\text{Li}, {}^6\text{Li}) {}^{65}\text{Zn}$ one-neutron ($1n$) transfer were also observed. One can see that the ΔE resolution was not good enough to separate completely ${}^7\text{Li}$ from ${}^6\text{Li}$.

In Fig. 2, experimental results for the ${}^7\text{Li} + {}^{64}\text{Zn}$ elastic scattering angular distribution at six incident energies are represented by circles (The different lines displayed in this

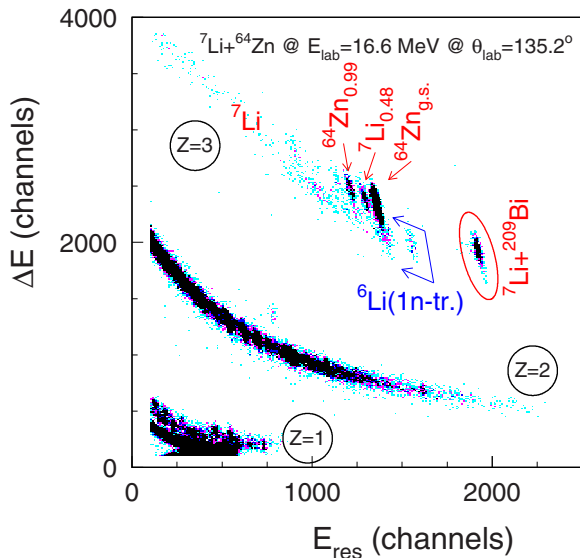


FIG. 1. (Color online) Two-dimensional ΔE - E_{res} spectrum measured at $E_{\text{lab}} = 16.6$ MeV, $\theta_{\text{lab}} = 135.2^\circ$.

figure are discussed in Sec. IV). The error bars in the figure represent statistical uncertainties only. The uncertainties in the cross sections due to the $1n$ -transfer “background” depend on the angle and on the beam energy and could amount up to $\sim 5\%$ at the highest measured angles at the highest energies.

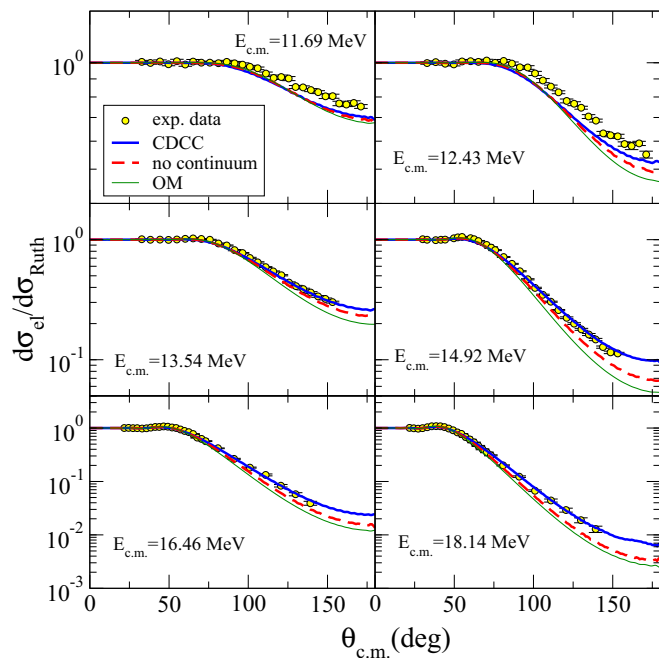


FIG. 2. (Color online) Elastic scattering angular distributions for the ${}^7\text{Li} + {}^{64}\text{Zn}$ system. The solid lines represent the CDCC calculations, the dashed lines are the calculations without the coupling to the continuum states and the thin lines represent the OM predictions without reorientation couplings (see Sec. IV for details).

III. CDCC CALCULATIONS

The CDCC formalism was proposed to extend the coupled-channel (CC) method for reactions induced by loosely bound systems, where the breakup channels can induce strong couplings to the continuum states of the projectile (see, e.g., Refs. [40,41]). Since continuum states are infinite and non-normalizable, a procedure of discretization is used, which allows to approximate this continuum by a finite set of square-normalizable states. For that purpose, the standard binning method was employed [41], which allows to discretize and include these unbound states in the calculations. The CDCC method has been successfully applied to study reactions induced by weakly bound nuclei, using three-body and four-body models of the reaction (see, e.g., Refs. [16–18,42–47]).

In this work, we consider a three-body model of the reactions ${}^6,7\text{Li} + {}^{64}\text{Zn}$, which is based on a $\alpha + d(t)$ model of ${}^6,7\text{Li}$ plus the ${}^{64}\text{Zn}$ target. The cluster separation energies for the systems $\alpha + d(t)$ are $S_\alpha = 1.47$ MeV and $S_\alpha = 2.47$ MeV, respectively. Due to such low separation energy, the coupling to the continuum states of the projectile is expected to be important. Therefore, these continuum states of the system $\alpha + d(t)$ are included and discretized by means of the binning method [41]. These calculations were performed using the code FRESKO [48], in which both nuclear and Coulomb effects were considered.

A. The ${}^6\text{Li}$ case

As was already mentioned, the ${}^6\text{Li}$ nucleus has an $\alpha + d$ cluster structure. The α - d binding potential of the Woods-Saxon form, taken from Ref. [49], was used to generate the 1^+ (angular momentum $\ell = 0$ coupled to the spin of the deuteron $s = 1$) ground state (g.s.) wave function; the potential depth has been adjusted to give the binding energy of 1.47 MeV. The same Woods-Saxon geometry was used for the resonant states 3^+ , 2^+ , and 1^+ ($\ell = 2$ coupled to the deuteron spin $s = 1$); the depth has been adjusted to reproduce the experimental energies of each of the resonances using the program GAMOW [50] (see Table I). The Coulomb potential of a uniformly charged sphere with radius R_C was included. The widths of the resonances calculated with this potential are compared with the experimental values of Ref. [2] in Table III.

In Ref. [51], the effect of nonresonant breakup states was shown to be quite significant. Thus, besides the resonant states, non-resonant continuum states with angular momentum $\ell = 0, 1$, and 2 were considered, where the same interaction α - d of the g.s. was used. The continuum states were truncated at 7 MeV and discretized into momentum bins of width 0.09 fm $^{-1}$.

TABLE I. Parameters of the Woods-Saxon potential corresponding to the α - d interaction. The Coulomb radius is $R_C = R$.

Potential	V (MeV)	R (fm)	a (fm)
α - d (g.s.)	77.47	1.9	0.65
α - d (3^+)	85.39	1.9	0.65
α - d (2^+)	75.27	1.9	0.65
α - d (1^+)	67.26	1.9	0.65

TABLE II. Parameters of the α - t potential.^a The Coulomb radius is $R_C = 3.095$ fm.

Potential	V (MeV)	α (fm ⁻²)	V_{SO} (MeV)
α - t (g.s., $1/2^-$)	83.52	0.15747	1.003
α - t ($7/2^-$)	83.52	0.15747	1.003
α - t ($5/2^-$)	78.19	0.15747	1.003

$$^a V(r) = -(V + 4\alpha V_{SO} \vec{\ell} \cdot \vec{\sigma}) \exp(-\alpha r^2).$$

These bins were modified for each resonance state; for the 3^+ , 2^+ , and 1^+ resonances the continuum discretization of 5.4 bins/MeV, 2.6 bins/MeV, and 2.8 bins/MeV was considered inside the resonance.

For the α - ^{64}Zn interaction, the Woods-Saxon parametrization of Ref. [4] was used. Besides the α - d and α - ^{64}Zn potentials, it is necessary to consider the interaction d - ^{64}Zn , which was obtained by single folding the p - ^{64}Zn plus n - ^{64}Zn interactions [52] over the deuteron g.s. wave function (see also Ref. [53]).

To obtain a good convergence, the wave function of the projectile-target relative motion was expanded in partial waves up to $J_{\text{max}} = 120$ and it was integrated numerically up to 70 fm.

B. The ^7Li case

The ^7Li nucleus can be well described by an $\alpha + t$ cluster structure. To obtain the bound states of ^7Li and the bin wave functions, the α - t potential of the Gaussian form, including central and spin-orbit terms, taken from Ref. [54] was used. The depth of the central potential has been adjusted to reproduce the experimental energies of each of the bound states, the $3/2^-$ g.s. and the $1/2^-$ first excited state ($\ell = 1$ coupled to the triton spin $s = 1/2$), and the unbound resonant states $7/2^-$ and $5/2^-$ ($\ell = 3$ coupled to the triton spin $s = 1/2$). As it can be seen from Table II, the bound states and the resonance $7/2^-$ can be reproduced by the same depth. This same potential was also used for the nonresonant continuum states of ^7Li . The calculated widths of the resonances are compared with the experimental values of Ref. [2] in Table III.

Continuum states with angular momentum $\ell = 0, 1, 2$, and 3 were considered, in which the $\ell = 3$ unbound states were modified in order to avoid double counting in the calculations. For the $5/2^-$ and $7/2^-$ resonances the continuum discretization of 1.25 bins/MeV and 1.43 bins/MeV was considered inside the resonance, while the nonresonant continuum was discretized in momentum bins of width 0.09 fm^{-1} up to 7 MeV.

The α - ^{64}Zn interaction of Ref. [4] was used, while for the interaction t - ^{64}Zn the parametrization of Ref. [55] was considered.

The number of partial waves of the projectile-target relative motion was limited to $J_{\text{max}} = 120$ and the integration was performed numerically up to 60 fm.

IV. RESULTS AND DISCUSSIONS

The calculated elastic scattering angular distributions for the ^7Li and ^6Li projectiles are represented by solid lines in

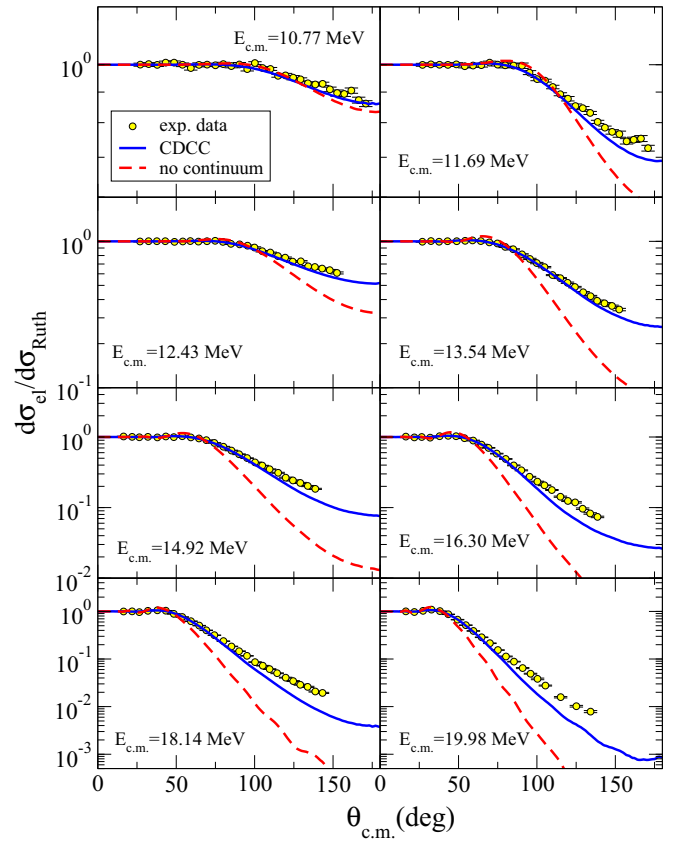


FIG. 3. (Color online) Elastic scattering angular distributions for the $^6\text{Li} + ^{64}\text{Zn}$ system. The solid lines represent the CDCC calculations, while the dashed lines are the calculations without the coupling to the continuum states.

Figs. 2 and 3, respectively. In general, a reasonable agreement with the experimental data is observed.

In the ^6Li case, the disagreements observed at highest energies are presumably due to the limitation of the two-body ($\alpha + d$) model of ^6Li . In Ref. [56], the $^6\text{Li} + ^{209}\text{Bi}$ elastic scattering was analyzed within three-body CDCC model and a good agreement with the experimental data was obtained by using normalization factors for the fragment-target potentials. On the other hand, it was shown in Ref. [53] that four-body CDCC calculations, based on a more realistic three-body ($\alpha + n + p$) model of ^6Li , reproduce the same data without renormalization of the potentials.

In the case of ^7Li , we can presume that the two-body $\alpha + t$ model works better since t is a stiffer particle than d due to its larger breakup threshold ($S_n = 6.26$ MeV [2] for $t \rightarrow d + n$). In Fig. 2, one can observe that the calculations slightly underestimate the experimental cross sections at the lowest energies. This disagreement could be due to the use of the global t - ^{64}Zn potential. We verified that a renormalization of this potential improves the agreement with the data and that the calculations are less sensitive to the α - ^{64}Zn potential.

In the same figures, the calculations without the coupling to the continuum states of the projectile are represented by dashed lines. The comparison between the two calculations and the

TABLE III. Resonant states of ${}^6\text{Li}$ (3^+ , 2^+ , and 1^+) and ${}^7\text{Li}$ ($7/2^-$ and $5/2^-$). The experimental energies E_{exp} and widths Γ_{exp} are taken from Ref. [2]. The widths Γ_{theo} are results of the program GAMOW [50].

Projectile	Resonance	E_{exp} (MeV)	Γ_{exp} (MeV)	Γ_{theo} (MeV)
${}^6\text{Li}$	3^+	0.716	0.024	0.018
${}^6\text{Li}$	2^+	2.84	1.3	0.85
${}^6\text{Li}$	1^+	4.18	1.5	2.36
${}^7\text{Li}$	$7/2^-$	2.16	0.093	0.092
${}^7\text{Li}$	$5/2^-$	4.21	0.88	0.90

experimental data reveals that the effect of the coupling to breakup channels is important in the case of the ${}^6\text{Li}$ projectile, while such effect has been found to be less significant in the ${}^7\text{Li}$ case. The calculations without breakup in the case of ${}^7\text{Li}$ include the g.s. reorientation couplings and the coupling to its bound $1/2^-$ first excited state. To evaluate the effects of these couplings, optical model (OM) calculations using only the bare interaction ${}^7\text{Li}(\text{g.s.})-{}^{64}\text{Zn}$, i.e., without reorientation couplings and excitation of the first excited state ($1/2^-$), have been performed. The potential ${}^7\text{Li}(\text{g.s.})-{}^{64}\text{Zn}$ is obtained by a single folding the $t-{}^{64}\text{Zn}$ plus $\alpha-{}^{64}\text{Zn}$ interactions over the $\alpha-t$ g.s. wave function. The results of the OM calculations are represented by thin green lines in Fig. 2. Notice that the reorientation couplings and the excitation of the ${}^7\text{Li}$ $1/2^-$ state have a significant effect in comparison with the couplings to breakup channels, mainly at medium measured energies. The g.s. reorientation couplings in ${}^6\text{Li}$ are absent since ${}^6\text{Li}(\text{g.s.})$ is a spherical nucleus.

To assess the effect of the coupling to the resonant states of ${}^6\text{Li}$ we have performed CDCC calculations including only the nonresonant continuum states, while the resonant states were ignored. This kind of calculations can be performed thanks to the bin procedure, which permits to remove or include the bins corresponding to the different resonant states. These resonant bins are determined by the energy and width of each resonance, presented in Table III.

In Fig. 4, the elastic scattering angular distributions for the ${}^6\text{Li} + {}^{64}\text{Zn}$ system at the four lower energies, $E_{\text{c.m.}} = 10.77$, 11.69, 12.43, and 13.54 MeV are shown. The solid lines represent the full CDCC calculations, the dashed lines are the calculations without the couplings to the continuum states, and the dotted lines represent the calculations considering only the nonresonant states. A comparison of these curves shows that inclusion of the couplings to the resonant states produces significant effect on the elastic scattering angular distributions at the lowest incident energies, while at higher energies these couplings become less important. At the lowest energies this effect improves considerably the agreement with the experimental data and is comparable to the effect of couplings to only non-resonant continuum. The dependence on the incident energy may be understood as an increment of the probability to access nonresonant continuum states with higher energies with respect to the resonant states.

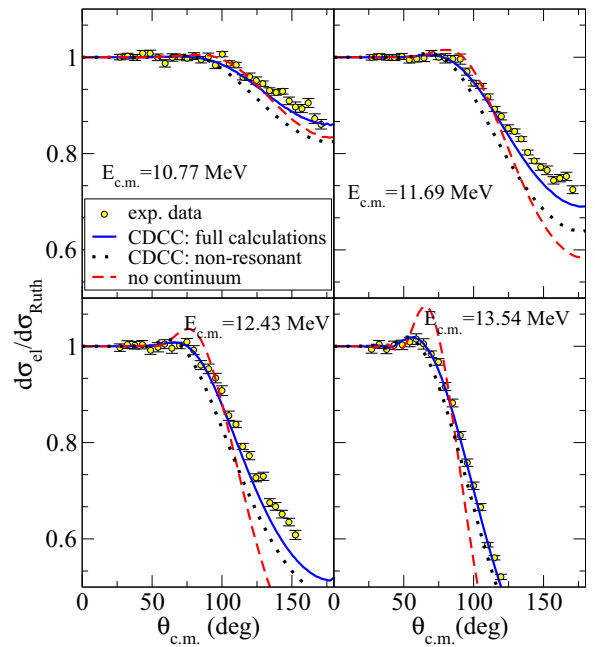


FIG. 4. (Color online) Elastic scattering angular distributions for the ${}^6\text{Li} + {}^{64}\text{Zn}$ system. The solid lines represent the CDCC calculations, the dotted lines are the calculations without the coupling to the resonant states, while the dashed lines are the calculations without the couplings to the continuum states.

In Ref. [57], similar calculations of the effect of couplings to resonant states on elastic scattering angular distributions were performed for the ${}^6\text{Li} + {}^{28}\text{Si}$ and ${}^6\text{Li} + {}^{58}\text{Ni}$ systems. It was found that the effect is negligible in the case of the ${}^{28}\text{Si}$ target, while some effect was observed at low energies in the case of the ${}^{58}\text{Ni}$ target. The effect of the resonant continuum states on the elastic scattering for the ${}^6\text{Li} + {}^{58}\text{Ni}$ system has a dependence on the incident energy as that observed in the present paper, becoming negligible when increasing the bombarding energy (see Fig. 4 in Ref. [57]). In the present case, the comparison between the calculations with and without the inclusion of couplings to resonant states is qualitatively similar to the one of Ref. [57], in which that effect was considered to be very small. However, it is clear from Fig. 4 that the inclusion of resonances has an important effect on the calculated cross sections for the ${}^6\text{Li} + {}^{64}\text{Zn}$ scattering at the lowest energies. Similar conclusion on the effect of the ${}^6\text{Li}$ resonances was also reached in Ref. [58] for the ${}^6\text{Li} + {}^{144}\text{Sm}$ system.

To study the importance of the coupling to the different resonant states of ${}^6\text{Li}$ we have performed CDCC calculations including the non-resonant continuum states and only one of the resonances, while the other resonant states were ignored. In Fig. 5, the elastic scattering angular distribution for the ${}^6\text{Li} + {}^{64}\text{Zn}$ system at $E_{\text{c.m.}} = 11.69$ MeV is shown. As before, the solid line represents the full CDCC calculation, while the calculations considering only the resonance 1^+ , 2^+ , or 3^+ are displayed by dotted, dashed, and dashed-dotted lines. One notes that the couplings to the 3^+ resonance are more relevant than to the 2^+ and 1^+ resonances. This can be understood

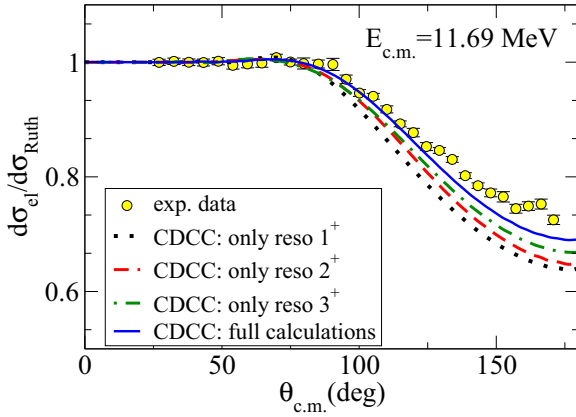


FIG. 5. (Color online) Elastic scattering angular distribution for the ${}^6\text{Li} + {}^{64}\text{Zn}$ system at $E_{\text{c.m.}} = 11.79$. Dotted, dashed, and dashed-dotted lines represent the CDCC calculations considering non-resonant states and only 1^+ , 2^+ , or 3^+ resonance, respectively. Full CDCC calculations are represented by solid lines.

given the lower excitation energy and narrower width of the 3^+ resonance compared to the other two.

Backscattering excitation functions and corresponding barrier distributions for the ${}^6, {}^7\text{Li} + {}^{64}\text{Zn}$ systems reported in Ref. [37] have been also analyzed with the CDCC method. In Ref. [37], in the case of the ${}^6\text{Li} + {}^{64}\text{Zn}$ system, the QEL scattering was defined as the sum of the elastic scattering and inelastic excitation of the ${}^{64}\text{Zn}$ 2^+ state. In the case of the ${}^7\text{Li} + {}^{64}\text{Zn}$ system, the inelastic excitation of the ${}^7\text{Li}$ $1/2^-$ state and $1n$ transfer to the ${}^{65}\text{Zn}$ states were also included in the QEL scattering. The transfer channel and the inelastic excitation of the target were not included in our CDCC calculations. Because of that, only the elastic scattering for ${}^6\text{Li} + {}^{64}\text{Zn}$ has been considered. In the case of ${}^7\text{Li} + {}^{64}\text{Zn}$, the elastic scattering and inelastic excitation of the ${}^7\text{Li}$ $1/2^-$ state have been analyzed.

The CDCC calculations of the backscattering cross sections were performed at the same energies, $E_{\text{lab}} = 9\text{--}20$ MeV in steps of 0.5 MeV, and angles, $\theta_{\text{lab}} = 160^\circ$ and 170° , for which the experimental cross sections were measured [37]. As in Ref. [37], the final backscattering excitation functions were obtained by correcting the center of mass energies $E_{\text{c.m.}}$ for the angle-dependent centrifugal potential and averaging the cross sections for the two angles. The barrier distributions were derived from the excitation functions using the same procedure [59] that was applied to the experimental data [37].

In Figs. 6 and 7, the calculated elastic scattering excitation functions and the corresponding barrier distributions, $D_{\text{qel}}^{\text{el}}$, are compared with the experimental data for the systems ${}^6\text{Li} + {}^{64}\text{Zn}$ and ${}^7\text{Li} + {}^{64}\text{Zn}$, respectively. Furthermore, the excitation function for the ${}^7\text{Li}(1/2^-)$ inelastic scattering and its component of the QEL barrier distribution, $D_{\text{qel}}^{\text{inel}}$, are also displayed in Fig. 7. A reasonable agreement between the experimental data and calculations is observed when the ${}^6, {}^7\text{Li} \rightarrow \alpha + d(t)$ resonant and nonresonant breakup processes are taken into account. In the ${}^6\text{Li}$ case, the effect of such couplings is to broaden the barrier distribution and to shift the

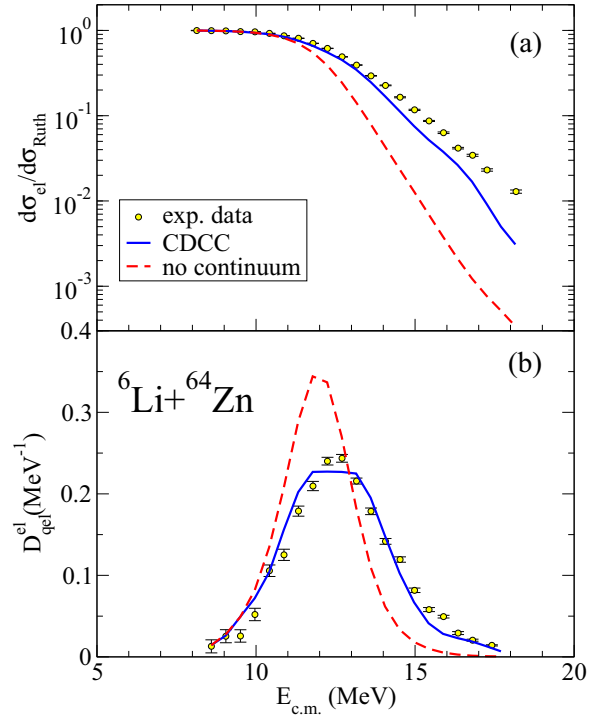


FIG. 6. (Color online) (a) Excitation function of elastic backscattering and (b) the corresponding contribution to the barrier distribution for ${}^6\text{Li} + {}^{64}\text{Zn}$ system. The experimental data are represented by the circles, while the solid lines correspond to the CDCC calculations. The dashed lines represent the calculations without the couplings to the continuum states.

barrier peak position to higher energies, while minor effects were observed in the case of ${}^7\text{Li}$.

To conclude, the comparison of the CDCC calculations with the experimental elastic angular distributions and barrier distributions show larger effect of the coupling to the breakup channels in a ${}^6\text{Li} + {}^{64}\text{Zn}$ system than in ${}^7\text{Li} + {}^{64}\text{Zn}$. The importance of these couplings was also reported for the total fusion and breakup cross sections at energies around the Coulomb barrier, for example in Refs. [60] and [61]. This behavior could be linked with the difference between the breakup thresholds, which is smaller for ${}^6\text{Li}$ (1.47 MeV) than for ${}^7\text{Li}$ (2.47 MeV).

Similar effects were observed for the ${}^6\text{Li}$ projectile with different targets in Ref. [16] and, recently, e.g., with ${}^{28}\text{Si}$ [62], ${}^{59}\text{Co}$ [63], ${}^{90}\text{Zr}$ [15], ${}^{144}\text{Sm}$ [35], ${}^{208}\text{Pb}$ [64], and ${}^{209}\text{Bi}$ [63], which support the results obtained in this work.

As it was shown in Fig. 6, the couplings to breakup channels can produce a shift of the barrier peak position to higher energies. This effect was also found for, e.g., ${}^6, {}^7\text{Li} + {}^{144}\text{Sm}$ [35] and ${}^6\text{Li} + {}^{28}\text{Si}$ [33, 62].

Thus, the results obtained in this work ratify that it is necessary to consider the couplings to breakup channels for a complete theoretical description of reactions induced by weakly bound projectiles. Moreover, it is found, in the case of the ${}^6\text{Li}$ projectile, that the effect of couplings to resonant states is important at low-incident energies.

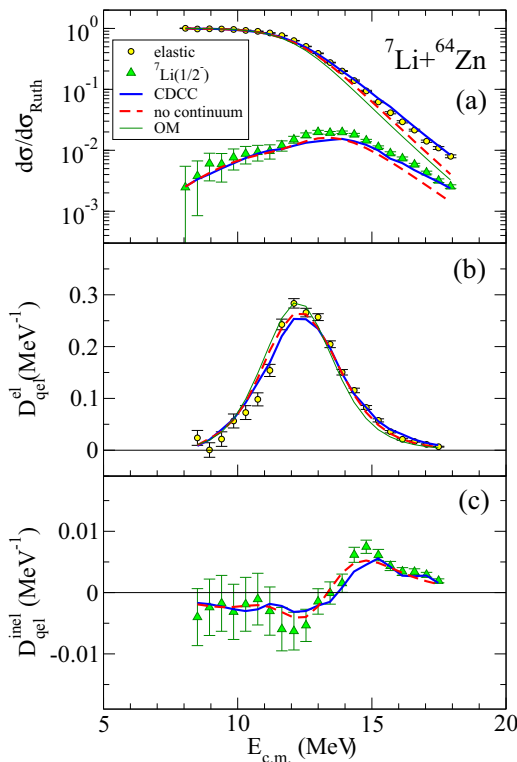


FIG. 7. (Color online) (a) Excitation functions of elastic and inelastic backscattering and the corresponding contributions to the QEL barrier distribution in (b) and (c), respectively, for ${}^7\text{Li} + {}^{64}\text{Zn}$ system. The experimental data are represented by the circles and triangles for the elastic and inelastic data, respectively. The solid lines correspond to the CDCC calculations, while the dashed lines represent the calculations without the couplings to the continuum states. The thin lines represent the OM without reorientation couplings.

V. SUMMARY AND CONCLUSIONS

We have measured elastic scattering angular distributions for the ${}^7\text{Li} + {}^{64}\text{Zn}$ system at energies around the Coulomb barrier in a wide angular range.

These new data, the elastic scattering angular distribution of ${}^6\text{Li} + {}^{64}\text{Zn}$ that we obtained in a previous experiment [36], our elastic backscattering excitation functions and their corresponding barrier distributions for both systems [37], have been compared with continuum-discretized coupled-channels calculations. The projectile dissociation has been taken into account by including the couplings to the $\alpha + d(t)$ resonant and non-resonant continuum states, while inelastic excitations of the target have not been considered.

In general, a good agreement between the calculations and the experimental data for both the elastic angular distributions and barrier distributions has been observed.

In the ${}^6\text{Li}$ case, the inclusion of resonant states has been found necessary to reproduce the experimental data at low energies. Moreover, a more important effect of the couplings to the 3^+ resonant state than to the 2^+ and 1^+ resonances has been observed; this is correlated with the excitation energies and widths of the resonances. The relative importance of the resonant continuum states with respect to nonresonant states decreases as the incident energy increases.

The couplings to the breakup channels have a significant effect in the case of the ${}^6\text{Li}$ scattering, whereas minor effects have been found for the ${}^7\text{Li}$ case. This behavior can be related to the fact that the breakup threshold of ${}^6\text{Li}$ is smaller than that of ${}^7\text{Li}$. Moreover, in the ${}^6\text{Li}$ case, those couplings tend to broaden the barrier distribution derived from elastic scattering and to increase its average energy.

The presented results confirm the importance of the coupling to the continuum in reactions involving weakly bound nuclei.

ACKNOWLEDGMENTS

O.G., V.O., and M.Z. would like to thank the LNS for the hospitality and financial support. A.M.M. is supported by the Spanish Ministerio de Economía y Competitividad, under Grant No. FIS2013-41994-P, by the Spanish Consolider-Ingenio 2010 Programme CPAN (CSD2007-00042), and by Junta de Andalucía (FQM160, P07-FQM-02894).

- [1] L. F. Canto, P. R. S. Gomes, R. Donangelo, and M. S. Hussein, Fusion and breakup of weakly bound nuclei, *Phys. Rep.* **424**, 1 (2006).
- [2] Evaluated Nuclear Structure Data File (NNDC, BNL, USA), <http://www.nndc.bnl.gov/ensdf/>.
- [3] I. J. Thompson and M. A. Nagarajan, Break-up effects in elastic scattering of ${}^6\text{Li}$ ions, *Phys. Lett. B* **106**, 163 (1981).
- [4] A. Di Pietro, P. Figuera, F. Amorini, C. Angulo, G. Cardella, S. Cherubini, T. Davinson, D. Leanza, J. Lu, H. Mahmud, M. Milin, A. Musumarra, A. Ninane, M. Papa, M. G. Pellegriti, R. Raabe, F. Rizzo, C. Ruiz, A. C. Shotton, N. Soić, S. Tudisco, and L. Weissman, Reactions induced by the halo nucleus ${}^6\text{He}$ at energies around the Coulomb barrier, *Phys. Rev. C* **69**, 044613 (2004).
- [5] A. Di Pietro, G. Randisi, V. Scuderi, L. Acosta, F. Amorini, M. J. G. Borge, P. Figuera, M. Fisichella, L. M. Fraile, J. Gomez-Camacho, H. Jeppesen, M. Lattuada, I. Martel, M. Milin, A. Musumarra, M. Papa, M. G. Pellegriti, F. Perez-Bernal, R. Raabe, F. Rizzo, D. Santonocito, G. Scalia, O. Tengblad, D. Torresi, A. M. Vidal, D. Voulot, F. Wenander, and M. Zadro, Elastic Scattering and Reaction Mechanisms of the Halo Nucleus ${}^{11}\text{Be}$ Around the Coulomb Barrier, *Phys. Rev. Lett.* **105**, 022701 (2010).
- [6] A. M. Sánchez-Benítez, D. Escrig, M. A. G. Alvarez, M. V. Andrés, C. Angulo, M. J. G. Borge, J. Cabrera, S. Cherubini, P. Demare, J. M. Espino, P. Figuera, M. Freer, J. E. García-Ramos, J. Gómez-Camacho, M. Gulino, O. R. Kakuee, I. Martel, C. Metelko, A. M. Moro, F. Pérez-Bernal, J. Rahighi, K. Rusek, D. Smirnov, O. Tengblad, P. Van Duppen, and V. Ziman, Study of the elastic scattering of ${}^6\text{He}$ on ${}^{208}\text{Pb}$ at energies around the Coulomb barrier, *Nucl. Phys. A* **803**, 30 (2008).
- [7] L. Acosta, A. M. Sánchez-Benítez, M. E. Gómez, I. Martel, F. Pérez-Bernal, F. Pizarro, J. Rodríguez-Quintero, K. Rusek, M. A. G. Alvarez, M. V. Andrés, J. M. Espino, J. P. Fernández-

- García, J. Gómez-Camacho, A. M. Moro, C. Angulo, J. Cabrera, E. Casarejos, P. Demaret, M. J. G. Borge, D. Escrig, O. Tengblad, S. Cherubini, P. Figuera, M. Gulino, M. Freer, C. Metelko, V. Ziman, R. Raabe, I. Mukha, D. Smirnov, O. R. Kakuee, and J. Rahighi, Elastic scattering and α -particle production in ${}^6\text{He} + {}^{208}\text{Pb}$ collisions at 22 MeV, *Phys. Rev. C* **84**, 044604 (2011).
- [8] M. Cubero, J. P. Fernández-García, M. Rodríguez-Gallardo, L. Acosta, M. Alcorta, M. A. G. Alvarez, M. J. G. Borge, L. Buchmann, C. A. Diget, H. A. Falou, B. R. Fulton, H. O. U. Fynbo, D. Galaviz, J. Gómez-Camacho, R. Kanungo, J. A. Lay, M. Madurga, I. Martel, A. M. Moro, I. Mukha, T. Nilsson, A. M. Sánchez-Benítez, A. Shotter, O. Tengblad, and P. Walden, Do Halo Nuclei Follow Rutherford Elastic Scattering at Energies Below the Barrier? The Case of ${}^{11}\text{Li}$, *Phys. Rev. Lett.* **109**, 262701 (2012).
- [9] N. Keeley, S. J. Bennett, N. M. Clarke, B. R. Fulton, G. Tungate, P. V. Drumm, M. A. Nagarajan, and J. S. Lilley, Optical model analyses of ${}^6\text{Li} + {}^{208}\text{Pb}$ elastic scattering near the Coulomb barrier, *Nucl. Phys. A* **571**, 326 (1994).
- [10] A. M. M. Maciel, P. R. S. Gomes, J. Lubian, R. M. Anjos, R. Cabezas, G. M. Santos, C. Muri, S. B. Moraes, R. L. Neto, N. Added, N. C. Filho, and C. Tenreiro, Influence of the ${}^6\text{Li}$ breakup process on the near barrier elastic scattering by heavy nuclei, *Phys. Rev. C* **59**, 2103 (1999).
- [11] P. R. S. Gomes, I. Padron, J. O. Fernández Niello, G. V. Martí, M. D. Rodríguez, O. A. Capurro, A. J. Pacheco, J. E. Testoni, A. Arazi, J. Lubian, R. M. Anjos, L. C. Chamon, E. Crema, and M. S. Hussein, Fusion, break-up and elastic scattering of weakly bound nuclei, *J. Phys. G* **31**, S1669 (2005).
- [12] M. S. Hussein, P. R. S. Gomes, J. Lubian, and L. C. Chamon, New manifestation of the dispersion relation: Breakup threshold anomaly, *Phys. Rev. C* **73**, 044610 (2006); **76**, 019902(E) (2007).
- [13] J. M. Figueira, J. O. Fernández Niello, D. Abriola, A. Arazi, O. A. Capurro, E. de Barbará, G. V. Martí, D. Martínez Heimann, A. E. Negri, A. J. Pacheco, I. Pádrón, P. R. S. Gomes, J. Lubian, T. Correa, and B. Paes, Breakup threshold anomaly in the elastic scattering of ${}^6\text{Li}$ on ${}^{27}\text{Al}$, *Phys. Rev. C* **75**, 017602 (2007).
- [14] M. Biswas, S. Roy, M. Sinha, M. K. Pradhan, A. Mukherjee, P. Basu, H. Majumdar, K. Ramachandran, and A. Shrivastava, The study of threshold behavior of effective potential for ${}^6\text{Li} + {}^{58,64}\text{Ni}$ systems, *Nucl. Phys. A* **802**, 67 (2008).
- [15] H. Kumawat, V. Jha, B. J. Roy, V. V. Parkar, S. Santra, V. Kumar, D. Dutta, P. Shukla, L. M. Pant, A. K. Mohanty, R. K. Choudhury, and S. Kailas, Breakup threshold anomaly in the elastic scattering for the ${}^6\text{Li} + {}^{90}\text{Zr}$ system, *Phys. Rev. C* **78**, 044617 (2008).
- [16] Y. Sakuragi, Energy and target dependence of projectile breakup effect in elastic scattering of ${}^6\text{Li}$, *Phys. Rev. C* **35**, 2161 (1987).
- [17] K. Rusek, N. Alamanos, N. Keeley, V. Lapoux, and A. Pakou, Breakup and fusion of ${}^6\text{Li}$ and ${}^6\text{He}$ with ${}^{208}\text{Pb}$, *Phys. Rev. C* **70**, 014603 (2004).
- [18] C. Beck, N. Keeley, and A. Diaz-Torres, Coupled-channel effects in elastic scattering and near-barrier fusion induced by weakly bound nuclei and exotic halo nuclei, *Phys. Rev. C* **75**, 054605 (2007).
- [19] D. R. Otomar, P. R. S. Gomes, J. Lubian, L. F. Canto, and M. S. Hussein, Nuclear and Coulomb breakup of the weakly bound ${}^6\text{Li}$ nucleus with targets in the range from $A = 59$ to 208, *Phys. Rev. C* **87**, 014615 (2013).
- [20] N. Rowley, G. R. Satchler, and P. H. Stelson, On the “distribution of barriers” interpretation of heavy-ion fusion, *Phys. Lett. B* **254**, 25 (1991).
- [21] M. Dasgupta, D. J. Hinde, N. Rowley, and A. M. Stefanini, Measuring barriers to fusion, *Annu. Rev. Nucl. Part. Sci.* **48**, 401 (1998).
- [22] H. Timmers, J. R. Leigh, M. Dasgupta, D. J. Hinde, R. C. Lemmon, J. C. Mein, C. R. Morton, J. O. Newton, and N. Rowley, Probing fusion barrier distributions with quasi-elastic scattering, *Nucl. Phys. A* **584**, 190 (1995).
- [23] N. Rowley, H. Timmers, J. R. Leigh, M. Dasgupta, D. J. Hinde, J. C. Mein, C. R. Morton, and J. O. Newton, Barrier distributions from elastic scattering, *Phys. Lett. B* **373**, 23 (1996).
- [24] H. Timmers, J. R. Leigh, N. Rowley, A. M. Stefanini, D. Ackermann, S. Beghini, L. Corradi, M. Dasgupta, J. H. He, D. J. Hinde, J. C. Mein, G. Montagnoli, C. R. Morton, J. O. Newton, F. Scarlassara, and G. F. Segato, Barrier distributions and scattering, *J. Phys. G* **23**, 1175 (1997).
- [25] C. J. Lin, H. Q. Zhang, F. Yang, M. Ruan, Z. H. Liu, Y. W. Wu, X. K. Wu, P. Zhou, C. L. Zhang, G. L. Zhang, G. P. An, H. M. Jia, and X. X. Xu, Effects of breakup of weakly bound projectile and neutron transfer on fusion reactions around Coulomb barrier, *Nucl. Phys. A* **787**, 281 (2007).
- [26] D. Patel, S. Mukherjee, B. K. Nayak, S. V. Suryanarayana, D. C. Biswas, E. T. Mirgule, Y. K. Gupta, L. S. Danu, B. V. John, and A. Saxena, Fusion barrier distributions in ${}^6\text{Li} + {}^{209}\text{Bi}$ reactions from quasi-elastic and fusion excitation function measurements, *Phys. Rev. C* **89**, 064614 (2014).
- [27] V. I. Zagrebaev, Understanding the barrier distribution function derived from backward-angle quasi-elastic scattering, *Phys. Rev. C* **78**, 047602 (2008).
- [28] D. S. Monteiro, P. R. S. Gomes, and J. Lubian, Interpretation of quasi-elastic barrier distributions for weakly bound systems, *Phys. Rev. C* **80**, 047602 (2009).
- [29] J. Lubian, T. Correa, P. R. S. Gomes, and L. F. Canto, Effect of breakup on fusion cross sections of the ${}^8\text{B} + {}^{58}\text{Ni}$ system by means of quasi-elastic angular distributions, *Phys. Rev. C* **78**, 064615 (2008).
- [30] Md. Moin Shaikh, S. Roy, S. Rajbanshi, M. K. Pradhan, A. Mukherjee, P. Basu, S. Pal, V. Nanal, R. G. Pillay, and A. Shrivastava, Barrier distribution functions for the system ${}^6\text{Li} + {}^{64}\text{Ni}$ and the effect of channel coupling, *Phys. Rev. C* **91**, 034615 (2015).
- [31] S. Mukherjee, B. K. Nayak, D. S. Monteiro, J. Lubian, P. R. S. Gomes, S. Appannababu, and R. K. Choudhury, Quasi-elastic scattering in the ${}^6\text{Li} + {}^{232}\text{Th}$ reaction, *Phys. Rev. C* **80**, 014607 (2009).
- [32] D. S. Monteiro, O. A. Capurro, A. Arazi, J. O. Fernández Niello, J. M. Figueira, G. V. Martí, D. M. Heimann, A. E. Negri, A. J. Pacheco, V. Guimarães, D. R. Otomar, J. Lubian, and P. R. S. Gomes, Near- and subbarrier elastic and quasielastic scattering of the weakly bound ${}^6\text{Li}$ projectile on ${}^{144}\text{Sm}$, *Phys. Rev. C* **79**, 014601 (2009).
- [33] K. Zerva, A. Pakou, K. Rusek, N. Patronis, N. Alamanos, X. Aslanoglou, D. Filipescu, T. Glodariu, N. Keeley, M. Kokkoris, M. La Commara, A. Lagoyannis, M. Mazzooco, N. G. Nicolis, D. Pierroutsakou, and M. Romoli, Probing the potential and reaction coupling effects of ${}^6\text{Li} + {}^{28}\text{Si}$ at sub- and near-barrier energies with elastic backscattering, *Phys. Rev. C* **82**, 044607 (2010).

- [34] K. Zerva, A. Pakou, N. Patronis, P. Figuera, A. Musumarra, A. Di Pietro, M. Fisichella, T. Glodariu, M. La Commara, M. Lattuada, M. Mazzocco, M. G. Pellegriti, D. Pierroutsakou, A. M. Sánchez-Benítez, V. Scuderi, E. Strano, and K. Rusek, Quasi-elastic backscattering of ${}^6,7\text{Li}$ on light, medium and heavy targets at near- and sub-barrier energies, *Eur. Phys. J. A* **48**, 102 (2012).
- [35] D. R. Otomar, J. Lubian, P. R. S. Gomes, D. S. Monteiro, O. A. Capurro, A. Arazi, J. O. Fernández Niello, J. M. Figueira, G. V. Martí, D. Martinez Heimann, A. E. Negri, A. J. Pacheco, V. Guimarães, and L. C. Chamon, Breakup coupling effects on near-barrier quasi-elastic scattering of ${}^6,7\text{Li}$ on ${}^{144}\text{Sm}$, *Phys. Rev. C* **80**, 034614 (2009).
- [36] M. Zadro, P. Figuera, A. Di Pietro, F. Amorini, M. Fisichella, O. Goryunov, M. Lattuada, C. Maiolino, A. Musumarra, V. Ostashko, M. Papa, M. G. Pellegriti, F. Rizzo, D. Santonocito, V. Scuderi, and D. Torresi, Elastic scattering of ${}^6\text{Li}$ on ${}^{64}\text{Zn}$ at near-barrier energies, *Phys. Rev. C* **80**, 064610 (2009).
- [37] M. Zadro, P. Figuera, A. Di Pietro, M. Fisichella, M. Lattuada, T. Lönnroth, M. Milin, V. Ostashko, M. G. Pellegriti, V. Scuderi, D. Stanko, E. Strano, and D. Torresi, Quasielastic backscattering and barrier distributions for the ${}^6,7\text{Li} + {}^{64}\text{Zn}$ systems, *Phys. Rev. C* **87**, 054606 (2013).
- [38] A. Di Pietro, P. Figuera, E. Strano, M. Fisichella, O. Goryunov, M. Lattuada, C. Maiolino, C. Marchetta, M. Milin, A. Musumarra, V. Ostashko, M. G. Pellegriti, V. Privitera, G. Randisi, L. Romano, D. Santonocito, V. Scuderi, D. Torresi, and M. Zadro, Heavy residue excitation functions for the collisions ${}^6,7\text{Li}$ near the Coulomb barrier, *Phys. Rev. C* **87**, 064614 (2013).
- [39] G. R. Satchler, Heavy-ion scattering and reactions near the Coulomb barrier and “threshold anomalies”, *Phys. Rep.* **199**, 147 (1991).
- [40] M. Kamimura, M. Yahiro, Y. Iseri, Y. Sakuragi, H. Kameyama, and M. Kawai, Chapter I. Projectile breakup processes in nuclear reactions, *Prog. Theor. Phys. Supp.* **89**, 1 (1986).
- [41] N. Austern, Y. Iseri, M. Kamimura, M. Kawai, G. Rawitscher, and M. Yahiro, Continuum-discretized coupled-channels calculations for three-body models of deuteron-nucleus reactions, *Phys. Rep.* **154**, 125 (1987).
- [42] T. Matsumoto, T. Kamizato, K. Ogata, Y. Iseri, E. Hiyama, M. Kamimura, and M. Yahiro, New treatment of breakup continuum in the method of continuum discretized coupled channels, *Phys. Rev. C* **68**, 064607 (2003).
- [43] J. A. Tostevin, F. M. Nunes, and I. J. Thompson, Calculations of three-body observables in ${}^8\text{B}$ breakup, *Phys. Rev. C* **63**, 024617 (2001).
- [44] D. J. Howell, J. A. Tostevin, and J. S. Al-Khalili, Coupled channels calculations of ${}^{11}\text{Be}$ breakup, *J. Phys. G* **31**, S1881 (2005).
- [45] M. Rodríguez-Gallardo, J. M. Arias, J. Gómez-Camacho, A. M. Moro, I. J. Thompson, and J. A. Tostevin, Four-body continuum-discretized coupled-channels calculations, *Phys. Rev. C* **80**, 051601(R) (2009).
- [46] J. P. Fernández-García, M. Rodríguez-Gallardo, M. A. G. Alvarez, and A. M. Moro, Long range effects on the optical model of ${}^6\text{He}$ around the Coulomb barrier, *Nucl. Phys. A* **840**, 19 (2010).
- [47] J. P. Fernández-García, M. Cubero, M. Rodríguez-Gallardo, L. Acosta, M. Alcorta, M. A. G. Alvarez, M. J. G. Borge, L. Buchmann, C. A. Diget, H. A. Falou, B. R. Fulton, H. O. U. Fynbo, D. Galaviz, J. Gómez-Camacho, R. Kanungo, J. A. Lay, M. Madurga, I. Martel, A. M. Moro, I. Mukha, T. Nilsson, A. M. Sánchez-Benítez, A. Shotter, O. Tengblad, and P. Walden, ${}^{11}\text{Li}$ Breakup on ${}^{208}\text{Pb}$ at Energies Around the Coulomb Barrier, *Phys. Rev. Lett.* **110**, 142701 (2013).
- [48] I. J. Thompson, Coupled reaction channels calculations in nuclear physics, *Comput. Phys. Rep.* **7**, 167 (1988).
- [49] K.-I. Kubo and M. Hirata, DWBA treatment of cluster transfer reactions, *Nucl. Phys. A* **187**, 186 (1972).
- [50] T. Vertse, K. F. Pál, and Z. Balogh, Gamow, a program for calculating the resonant state solution of the radial Schrödinger equation in an arbitrary optical potential, *Comput. Phys. Commun.* **27**, 309 (1982).
- [51] Y. Hirabayashi, Effects of nonresonant breakup states in polarized ${}^6\text{Li}$ scattering, *Phys. Rev. C* **44**, 1581 (1991).
- [52] A. J. Koning and J. P. Delaroche, Local and global nucleon optical models from 1 KeV to 200 MeV, *Nucl. Phys. A* **713**, 231 (2003).
- [53] S. Watanabe, T. Matsumoto, K. Minomo, K. Ogata, and M. Yahiro, Effects of four-body breakup on ${}^6\text{Li}$ elastic scattering near the Coulomb barrier, *Phys. Rev. C* **86**, 031601(R) (2012).
- [54] B. Buck and A. C. Merchant, Cluster model of $A = 7$ nuclei revisited, and the astrophysical S factors for ${}^3\text{He}(\alpha, \gamma) {}^7\text{Be}$ and ${}^3\text{H}(\alpha, \gamma) {}^7\text{Li}$ at zero energy, *J. Phys. G* **14**, L211 (1988).
- [55] F. D. Becchetti Jr. and G. W. Greenlees, Annual Report J. H. Williams Laboratory, University of Minnesota, 1969.
- [56] N. Keeley, J. M. Cook, K. W. Kemper, B. T. Roeder, W. D. Weintraub, F. Maréchal, and K. Rusek, Effect of $e1$ excitations to the continuum: ${}^6\text{He}$ and ${}^6\text{Li} + {}^{209}\text{Bi}$ compared, *Phys. Rev. C* **68**, 054601 (2003).
- [57] A. Gómez Camacho, A. Diaz-Torres, P. R. S. Gomes, and J. Lubian, Effect of ${}^6\text{Li}$ resonances on near-barrier elastic scattering involving ${}^{28}\text{Si}$ and ${}^{58}\text{Ni}$ target nuclei, *Phys. Rev. C* **91**, 014607 (2015).
- [58] A Gómez-Camacho, CDCC calculations of elastic scattering for the systems ${}^6\text{Li} + {}^{144}\text{Sm}$ and ${}^6\text{Li} + {}^{208}\text{Pb}$. Effect of resonances of ${}^6\text{Li}$ on elastic scattering angular distributions, *J. Phys.: Conf. Ser.* **578**, 012003 (2015).
- [59] O. A. Capurro, J. E. Testoni, D. Abriola, D. E. DiGregorio, G. V. Martí, A. J. Pacheco, M. R. Spinella, and E. Achterberg, Barrier distributions derived from quasielastic excitation functions for the ${}^{12,13}\text{C} + {}^{105,106}\text{Pd}$ systems, *Phys. Rev. C* **62**, 014613 (2000).
- [60] N. Keeley and K. Rusek, Near-barrier polarization potentials for ${}^6,7\text{Li} + {}^{208}\text{Pb}$, *Phys. Lett. B* **427**, 1 (1998).
- [61] M. Dasgupta, D. J. Hinde, K. Hagino, S. B. Moraes, P. R. S. Gomes, R. M. Anjos, R. D. Butt, A. C. Berriman, N. Carlin, C. R. Morton, J. O. Newton, and A. Szanto de Toledo, Fusion and breakup in the reactions of ${}^6\text{Li}$ and ${}^7\text{Li}$ nuclei with ${}^{209}\text{Bi}$, *Phys. Rev. C* **66**, 041602(R) (2002).
- [62] K. Zerva, N. Patronis, A. Pakou, N. Alamanos, X. Aslanoglou, D. Filipescu, T. Glodariu, M. Kokkoris, M. La Commara, A. Lagoyannis, M. Mazzocco, N. G. Nicolis, D. Pierroutsakou, M. Romoli, and K. Rusek, Elastic backscattering measurements for ${}^6\text{Li} + {}^{28}\text{Si}$ at sub- and near-barrier energies, *Phys. Rev. C* **80**, 017601 (2009).
- [63] A. Diaz-Torres, I. J. Thompson, and C. Beck, How does breakup influence the total fusion of ${}^6,7\text{Li}$ at the Coulomb barrier?, *Phys. Rev. C* **68**, 044607 (2003).
- [64] G. R. Kelly, N. J. Davis, R. P. Ward, B. R. Fulton, G. Tungate, N. Keeley, K. Rusek, E. E. Bartosz, P. D. Cathers, D. D. Caussyn, T. L. Drummer, and K. W. Kemper, α breakup of ${}^6\text{Li}$ and ${}^7\text{Li}$ near the Coulomb barrier, *Phys. Rev. C* **63**, 024601 (2000).